On the generation of the mean velocity profile for turbulent boundary layers with pressure gradient under equilibrium conditions

A. Rona[a], M. Grottadaurea[a], M. Monti[a], C. Airiau[b,c], T. Gandhi[b,c]

[a] *Department of Engineering, University of Leicester, University Road, Leicester, LE1 7RH, UK*
[b] *Université de Toulouse; INPT, UPS; IMFT (Institut de Mécanique des Fluides de Toulouse), Allée Camille Soula, F-31400 Toulouse, France*
[c] *CNRS; IMFT; F-31400 Toulouse, France*

Abstract

The generation of a fully turbulent boundary layer profile is investigated using analytical and numerical methods over the Reynolds number range $300 \leq Re_\theta \leq 31000$. The predictions are validated against reference wind tunnel measurements under zero streamwise pressure gradient. The analytical method is then tested for a low and moderate adverse pressure gradient. Comparison against experimental and DNS data show a good predictive ability under a zero pressure gradient and a moderate adverse pressure gardient, with the numerical method providing a complete velocity profile through the laminar sub-layer down to the wall. The application of the method is useful to computational fluid dynamic practitioners for generating an equilibrium thick turbulent boundary layer at the computational domain inflow.

Key words:

Nomenclature

A	Integration constant for the outer region velocity profile
B	Logarithmic law constant
C	Logarithmic law constant for the inner region
C_2	Non-dimensional momentum thickness
C_f	Skin friction coefficient
c_ℓ	Normalized mixing length at $y \to \delta$
D_v	Logarithmic law constant for the outer region
$\tilde{\mathrm{F}}$	Van Driest near wall damping correction
F	Normalized defect velocity, $u_e^+ - u^+$

Email addresses: ar45@le.ac.uk (A. Rona), mg165@le.ac.uk (M. Grottadaurea), mm295@le.ac.uk (M. Monti), airiau@imft.fr (C. Airiau), gandhi@imft.fr (T. Gandhi)

H	Shape factor
K	Sink flow acceleration parameter
L	Flat plate length
ℓ	Mixing length
N	Number of data points in the experimental velocity profile
p	Pressure
Q	Potential sink strength
$\Re$	Real number
Re	Reynolds number
T	Temperature
u	Tangential velocity
u_τ	Friction velocity
x	Tangential distance from the boundary layer leading edge
y	Wall-normal distance from the solid wall
α	Outer region normalized displacement thickness
β	Normalized streamwise pressure gradient
$\tilde{\beta}$	Non-dimensional free-stream acceleration parameter, $\tilde{\beta} = 2\beta F_1$
β_c	Clauser parameter
δ	Boundary layer thickness
δ^*	Boundary layer displacement thickness
ϵ	Least squares error
η	Outer layer non-dimensional coordinate, $\eta = y/\delta$
θ	Boundary layer momentum thickness
κ	von Karman constant, $\kappa = 0.41$
λ	Local free-stream to leading edge free-stream velocity ratio, u_e/u_0
μ_l	Laminar or molecular viscosity
ν	Kinematic viscosity
Π	Wake parameter
ρ	Density
τ	Tangential shear stress
Subscripts	
a	Analytical prediction
e	Free-stream condition
ex	Experimental value
l	Laminar component
n	Result numerically obtained
s	Direct Numerical Simulation value
t	Reynolds average (turbulent) component
w	Wall condition
0	Leading edge condition
Superscripts	
$+$	Inner layer scaling
$\bar{()}$	Time average
$\prime$	Fluctuation about the time-mean value

1. Introduction

Computational fluid dynamic simulations of wall bounded flows, such as the flow over high-lift devices, ailerons, the elevators and the rudder, often use a turbulent boundary layer inflow to reduce the computational domain size with respect to a full wing, tailplane or fin simulation. The quality of the numerical predictions can be significantly affected by how well the boundary layer inflow is modelled. This paper compares the use of analytical correlations and of an auxiliary boundary layer numerical method to generate a turbulent boundary layer inflow for CFD over a wide Reynolds number range.

Computational fluid dynamic simulations of individual airframe components are commonly used to study the local aerodynamics in details [1, 2, 3]. This enables to achieve a sufficient level of spatial and temporal refinement around the specific components to model the onset of self-sustained oscillations, such as those in cavity flows, edge tones and other fluid-resonant geometries. These flow instabilities contribute to airframe noise and a good quality inflow prediction is very important to achieve quantitative predictions of the radiated noise pattern. For instance, in a cavity, the inflow momentum thickness has a direct influence on acoustic mode selection [4].

Where the inflow features a fully developed turbulent boundary layer, an analytical profile for the mean velocity can be imposed, derived from the integral boundary layer parameters as determined from either a larger-scale numerical simulation or from experiment. A common choice for specifying the boundary layer inflow in aerodynamics is by defining the inflow free-stream velocity u_e, temperature T_e, pressure p_e, boundary layer thickness δ, momentum thickness based Reynolds number Re_θ, shape factor H, and the streamwise pressure gradient dp_e/dx.

An alternative approach to define the mean velocity inflow is by using an auxiliary numerical simulation of the upstream boundary layer obtained, for instance, from running two-dimensional companion software by Wilcox [5].

This paper presents and validates one analytical and one numerical approach for generating a turbulent boundary layer inflow in CFD. The analytical method is a variant of the defect law by Coles [6], while the numerical method is derived from matched asymptotic expansions [7]. The analytical approach is then applied to a boundary layer with adverse pressure gradient.

Section 2.1 details the analytical method used to generate the outer layer velocity profile in a turbulent boundary layer. Section 2.2 details the numerical method based on the equilibrium boundary layer model. Section 3 validates both methods using zero pressure gradient velocity data over the Reynolds number range $300 \leq Re_\theta \leq 31000$. Section 4 extends the validation to the adverse pressure gradient boundary layer and presents sensitivity analysis on the mixing length parameter.

2. Method description and elements of the mixing length model

2.1. Analytical method

To describe the mean velocity profile in a turbulent boundary layer, similarity solutions are sought in the inner and the outer regions. In the inner region, the mean streamwise velocity u scales with the wall friction velocity u_τ and with the viscous length scale $l = \nu_l/u_\tau$, so that

$$\frac{u}{u_\tau} = f\left(y^+\right) \tag{1}$$

where $y^+ = yu_\tau/\nu_l$ is the inner scaling non-dimensional wall-normal distance. In outer region, the velocity profile is described by the velocity defect law

$$\frac{u_e - u}{u_\tau} = f\left(\eta\right) \tag{2}$$

where $\eta = y/\delta$ is the outer scaling non-dimensional wall-normal distance, u_e is the free-stream velocity, ν_l is the laminar kinematic viscosity, y is the wall-normal distance and δ is the boundary layer thickness, which is taken as the wall-normal distance at which $u = u_e$.

Based on the existence of an overlap region between the inner and the outer regions, Coles [6] proposed the following additive law of the wall and law of the wake in non-dimensional form:

$$\begin{aligned} u^+ &= \frac{1}{\kappa}\ln y^+ + B + \frac{\Pi}{\kappa} f\left(\eta\right) \\ f\left(\eta\right) &= 1 - \cos\left(\pi\eta\right) \end{aligned} \tag{3}$$

where $u^+ = u/u_\tau$ is the normalized streamwise velocity, Π is the wake parameter, κ the von Kármán constant, and B the logarithmic law constant.

Coles [6] determined the wake parameter as

$$\Pi = \kappa/2\left(u_e^+ - \kappa^{-1}\ln Re_\tau - B\right) \tag{4}$$

where $Re_\tau = \delta u_\tau/\nu_l$ is the boundary layer Reynolds number and $u_e^+ = u_e/u_\tau$ is the normalized free-stream velocity.

Let

$$f\left(\eta\right) = A_1\eta^2 + A_2\eta^3 \tag{5}$$

be a cubic polynomial approximation to $f\left(\eta\right)$ in eq. 3. Substituting the boundary conditions

$$u\big|_{y=\delta} = u_e \tag{6}$$

and

$$\left.\frac{\partial u}{\partial y}\right|_{y=\delta} = 0 \tag{7}$$

in eq. 3, with $f(\eta)$ from eq. 5, gives $A_1 = 6\,[1 + 1/(6\Pi)]$ and $A_2 = -4\,[1 + 1/(4\Pi)]$, with Π defined by eq. 4. The law of the wake of eq. 3 then becomes

$$u^+ = \underbrace{\overbrace{\frac{1}{\kappa}\ln y^+ + B}^{\text{Log-law of the wall}} + \frac{1}{k}\eta^2\,(1-\eta)}_{\text{Pure wall flow}} \quad \underbrace{+2\frac{\Pi}{\kappa}\eta^2\,(3-2\eta)}_{\text{Pure wake component}} \tag{8}$$

Equation 8 is validated over a relatively wide range of momentum thickness based Reynolds number $Re_\theta = u_e\theta/\nu_l$ in section 3. To evaluate eq. 8, the authors take $\kappa = 0.41$ and $B = 5.0$, as proposed by Coles [6].

2.2. Successive complementary expansion method

The successive complementary expansion method consists in seeking contiguous asymptotic matches between the inner and the outer regions of an incompressible turbulent boundary layer. This approach is detailed in Cousteix & Mauss [7] and this paper only reproduces the key steps that support the authors' application to turbulent boundary layers.

2.3. Mixing length model

Across the boundary layer, the local shear stress

$$\tau = \mu_l\frac{\partial u}{\partial y} - \rho\overline{u'v'} = \tau_l + \tau_t \tag{9}$$

where u' and v' are the time-dependent fluctuations of the streamwise and flow-normal velocity components and are unknown. To avoid having to resolve these unknowns, the Reynolds shear stress τ_t is evaluated using Prandtl's mixing length model [8], with the Van Driest [9] near-wall damping correction $\tilde{\mathrm{F}}$. This gives

$$\tau_t = \rho\tilde{\mathrm{F}}^2\ell^2\left|\frac{\partial u}{\partial y}\right|\left(\frac{\partial u}{\partial y}\right) \tag{10}$$

where $\tilde{\mathrm{F}} = 1 - \exp(-y^+/26)$.

In the inner region, $\ell = \kappa y$, while in the outer region, $\ell/\delta \to c_\ell$ as $y \to \delta$ and $c_\ell = 0.085$. These two trends can be merged analytically into a single distribution for the mixing length ℓ across the full boundary layer by the use of a blending function. Michel et al. [10] used the blending function

$$\ell(\eta) = \delta c_\ell \tanh(\frac{\kappa\eta}{c_\ell}) \tag{11}$$

with $\kappa = 0.41$. The authors propose an alternative blending function that is shown in section 3 to give an improved prediction of the turbulent shear stress profile at the interface between the inner and the outer layer, at low Reynolds numbers Re_τ. This is

$$\ell(\eta) = \delta\frac{\kappa\eta}{\left[1 + (\kappa\eta/c_\ell)^n\right]^{1/n}} \tag{12}$$

For $2.6 < n < 2.7$, the $\ell(\eta)$ profile from equation 12 almost matches that from equation 11.

2.4. The defect law and the wall sub-layer

2.4.1. Inner region velocity profile

Normalising the local shear stress τ in eq. 10 by ρu_τ^2 and assuming a monotonic velocity profile gives

$$\frac{\tau}{\tau_w} = \frac{\partial u^+}{\partial y^+} + \ell^{+2}\tilde{\mathrm{F}}^2 \left(\frac{\partial u^+}{\partial y^+}\right)^2 \tag{13}$$

where $\ell^+ = \ell u_\tau/\nu_l$. In the limit $y^+ \to 0$, $\tau \to \tau_w$ and eq. 13 becomes

$$1 = \frac{\partial u^+}{\partial y^+} + \ell^{+2}\tilde{\mathrm{F}}^2 \left(\frac{\partial u^+}{\partial y^+}\right)^2 \tag{14}$$

Equation 14 is a quadratic in $\partial u^+/\partial y^+$ with root [7]

$$\frac{\partial u^+}{\partial y^+} = \frac{2}{1 + \sqrt{1 + 4\left[\ell^+\left(y^+\right)\tilde{\mathrm{F}}\left(y^+\right)\right]^2}} \tag{15}$$

Integrating equation 15 with respect to y^+ with the boundary condition $u^+(x,0) = 0$ gives the inner layer tangential velocity profile that asymptotes to the log-law of the wall in equation 8 for $y^+ > 80$ with $B = 5.28$.

2.4.2. Outer region velocity profile

In an equilibrium turbulent boundary layer, a similarity solution for the outer layer is sought in terms of the velocity defect $F'(\eta) = u_e^+ - u^+$, under the local assumption of no boundary layer growth. Expressing τ/τ_w as a function of F and η gives [7]

$$\tau^+ = \frac{\tau}{\tau_w} = 1 - \frac{F}{F_1} + \left(\frac{1}{F_1} + 2\beta\right)\eta F' \tag{16}$$

where

$$F = \int_0^\eta F'(\xi)\, d\xi; \quad F_1 = F(1); \quad \beta = -\frac{\delta}{u_\tau}\frac{du_e}{dx} \tag{17}$$

In the outer region, the Reynolds stress component is dominant over the laminar shear stress, so $\tau \simeq \tau_t$.

From eq. 10, noting that the Van Driest damping constant $\tilde{\mathrm{F}} \to 1$ at $y^+ \geq 100$, $\tau/\tau_w = (\ell/\delta)^2 F''^2$, where $F'' = dF'/d\eta$. Substituting for τ/τ_w in eq. 16, the similarity solution for the outer region becomes

$$\left(\frac{\ell}{\delta}\right)^2 F''^2 = 1 - \frac{F}{F_1} + \left(\frac{1}{F_1} + 2\beta\right)\eta F' \tag{18}$$

2.4.3. Asymptotic matching of the inner and outer profiles

A matching condition is sought for the velocity profiles of the inner and outer regions, equations 15 and 18. This is obtained from standard asymptotic analysis [7] by considering eq. 15 in the limit $y^+ \to \infty$ and eq. 18 in the limit $\eta \to 0$ that give respectively [7]

$$u^+ = \kappa^{-1} \ln y^+ + C \tag{19}$$

$$u_e^+ - u^+ = -\kappa^{-1} \ln \eta + D_v \tag{20}$$

Adding eq. 19 to eq. 20 gives [7]

$$u_e^+ = \kappa^{-1} \ln \frac{u_\tau \delta}{\nu_l} + C + D_v \tag{21}$$

Equation 21 can be re-cast as function of the wall skin friction coefficient $C_f = \tau_w / \left(0.5 \rho u_e^2\right)$ that is imposed as equal in the inner and outer regions and provides the matching criterion for the two profiles at $Re_\tau = u_\tau \delta / \nu_l$

$$\sqrt{\frac{2}{C_f}} = \kappa^{-1} \ln Re_\tau + C + D_v \tag{22}$$

2.5. Numerical implementation

Expliciting the outer region velocity profile poses several challenges. Equation 18 is non-linear and is ill-defined at the upper boundary layer limit, at $\eta \to 1$, where $F'' \to 0$, and at the lower boundary layer limit, at $\eta \to 0$, where $\ell/\delta \to 0$ and $F'' \to \infty$. To solve the problem, auxiliary approximate solutions are imposed on the floor of the laminar sub-layer and at the edge of the boundary layer, as shown in figure 1, so that the edges of the inner and of the outer regions are modelled analytically while the overlap region is resolved numerically.

Let $f(\eta) = F(\eta)/F(1)$. On the floor of the laminar sub-layer, imposing $\eta = 0$ and $\ell = \kappa y$, as in section 2.3, eq. 18 becomes

$$\left[\kappa \eta F_1 f''(\eta)\right]^2 = 1 - f(\eta) + (1 + 2\beta F_1)\, \eta f'(\eta) \tag{23}$$

with the boundary condition $f(0) = 0$. Let introduce the term

$$\tilde{\beta} = 2\beta F_1 \tag{24}$$

This term allows the model to account for the presence of non-zero pressure gradients if $\beta \neq 0$.

In a zero pressure gradient boundary layer, $\beta = 0$ by eq. 17, for which eq. 23 has the explicit solution

$$f(\eta) = \frac{\eta^2}{4\alpha^2} - \frac{\eta \ln \eta}{\alpha} + A\, \eta; \quad f'(\eta) = \frac{\eta}{2\alpha^2} - \frac{1 + \log \eta}{\alpha} + A; \quad f''(\eta) = \frac{1}{2\alpha^2} - \frac{1}{\alpha \eta}$$

with $\alpha = F_1 \kappa$. The integration constant A is determined by evaluating $f'(\eta)$ at $\eta = \epsilon_0$ on the floor of the laminar sub-layer. In a non-zero pressure gradient

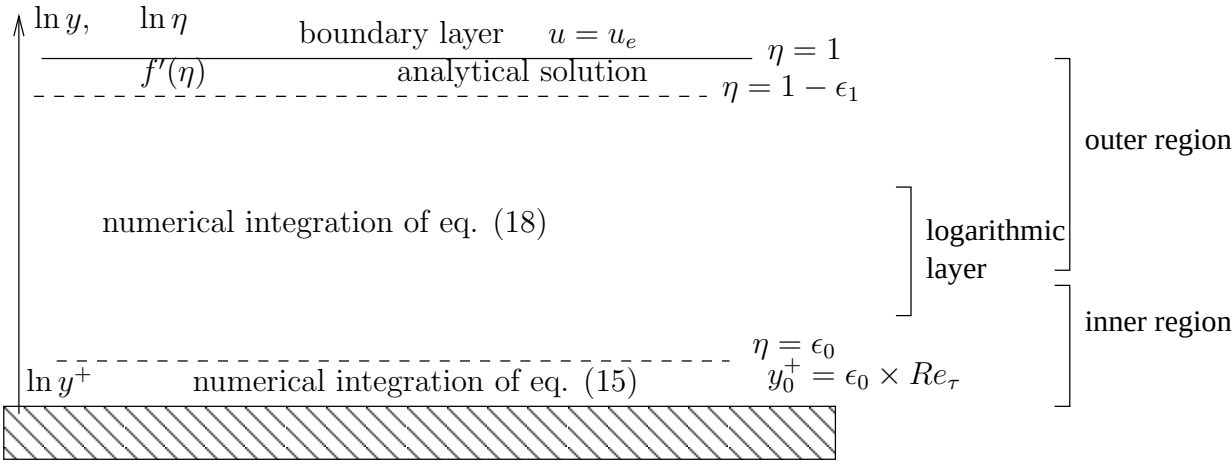

Figure 1: Boundary layer decks.

boundary layer, $\tilde{\beta}\eta f' \to 0$ as $\eta \to 0$. The term β has a weak influence approaching the wall, hence the zero pressure gradient profile is used on the floor of the laminar sub-layer for all β.

At the edge of the boundary layer, at $\eta = 1$, eq. 18 becomes

$$\left[\ell_1 F_1 f''(\eta)\right]^2 = 1 - f(\eta) + \left(1 + \tilde{\beta}\right)\eta f'(\eta) \tag{25}$$

with the boundary conditions $f(1) = 1$, $f'(1) = 0$, $f''(1) = 0$ and ℓ_1 evaluated from eq. 12 at $\eta = 1$. Cousteix [11] proposed the solution for eq. 25

$$f(\eta) = 1 - \frac{(1-\eta)^3}{3}; \quad f'(\eta) = (1-\eta)^2; \quad f''(\eta) = -2 + 2\eta \tag{26}$$

for $\beta = 0$, that has the attractive property of being independent from F_1 and ℓ_1 and is the solution used in this work. The same solution is used for $\beta \neq 0$, as $\tilde{\beta}\eta f'(\eta) = 0$ by the boundary condition $f'(1) = 0$ in eq. 25.

An additional difficulty is introduced from $\beta \neq 0$. The term βF_1 is infact unknown a priori since F_1 can be evaluated from the solution of the problem only if β is initially fixed. As F_1 is a problem output, eq. 24 can be solved using a standard Newton-Raphson method. Let guess a value for $\tilde{\beta}$, the relative value of the pressure gradient β of the problem can be determinated by iterating

$$\beta(\tilde{\beta}_n + \Delta\tilde{\beta}_n) = \beta(\tilde{\beta}_n) + \frac{d\beta}{d\tilde{\beta}}\Delta\tilde{\beta}_n = \beta_{\text{target}} \Longrightarrow \quad \Delta\tilde{\beta}_n = 2F_1(\beta_{\text{target}} - \beta(\tilde{\beta}_n)) \tag{27}$$

until convergence.

Re_θ	Re_τ	u_e^+	Π	$100 \times \epsilon$	Symbol	$(Re_\tau)_\mathrm{n}$	$(u_e^+)_\mathrm{n}$	$100 \times \epsilon_\mathrm{n}$
300	145	18.25	0.228	1.33	$\circ$	142	18.54	2.12
697	335	20.25	0.219	1.35	$*$	315	20.77	3.31
1003	460	21.5	0.317	1.78	$\triangle$	446	21.66	2.39
1430	640	22.4	0.336	1.38	$\cdot$	627	22.51	2.77
2900	1192	24.33	0.421	1.02	$\triangleleft$	1240	24.17	2.48
3654	1365	25.38	0.568	0.72	$\times$	1551	24.71	2.44
5200	2000	26	0.505	1.62	$\triangleright$	2185	25.54	2.38
12633	4436	28.62	0.643	0.71	$\square$	5188	27.65	2.51
13000	4770	28	0.480	0.99	$\diamond$	5335	27.72	1.84
22845	8000	30.15	0.662	1.01	$+$	9258	29.06	2.34
31000	13030	30	0.388	2.05	$\star$	12845	29.79	1.86

Table 1: Experimental velocity profiles.

DNS	β_c	Re_θ	Re_τ	u_s^+	Π	$100 \times \epsilon$	Symbol	$(Re_\tau)_\mathrm{n}$	$(u_e^+)_\mathrm{n}$	$100 \times \epsilon_\mathrm{n}$
ZPG1	0	422	222	19.54	0.298	0.39	$\triangledown$	220	19.8	1.33
ZPG2	0	588	272	20.45	0.385	0.32	$\hexagram$	270	20.5	0.25

Table 2: DNS velocity profiles at zero pressure gradient. Right-hand side of the table : $n = 4$ in equation 12.

3. The zero pressure gradient boundary layer

3.1. Analytical, numerical and experimental velocity profiles

The analytical and numerical methods for predicting a boundary layer mean turbulent velocity profile are tested against a range of streamwise velocity measurements of zero pressure gradient boundary layers [12, 13, 14, 15] over the range $300 \leq Re_\theta \leq 31000$. Table 1 lists the values of u_e^+, Re_τ and Π at each Re_θ of the experimental velocity traverse records [12, 13, 14, 15]. The values of u_e^+ and Re_τ are the ones reported in experiment [12, 13, 14, 15] while Π has been obtained by fitting eq. 8 using the least squares fit. The normalized mean streamwise velocity u^+ is plotted against the normalized wall-normal distance y^+ in figure 2 for different Reynolds numbers. The symbols used in figure 2 are measured values [12, 13, 14, 15] at different Re_θ, labelled as in table 1. The continuous lines show the fitted analytical profiles for the outer layer. For clarity, an incremental shift of $u^+ = 2.5$ is applied to all curves.

3.2. Analytical, numerical and Direct Numerical Simulation velocity profiles

The normalized mean streamwise velocity u^+ profiles from the analytical method are further tested against Direct Numerical Simulations of zero pressure gradients boundary layers at two different Re_θ. The parameters of the DNS work [16] are in table 2. The values of u_s^+ and Re_τ are the ones reported in the numerical work while Π has been obtained by fitting eq. 8 using the least squares fit. The two analytical profiles at $Re_\theta = 422$ (red dashed line) and $Re_\theta = 588$ (blue dashdotted line) are shown in between the experimental profiles in figure 3

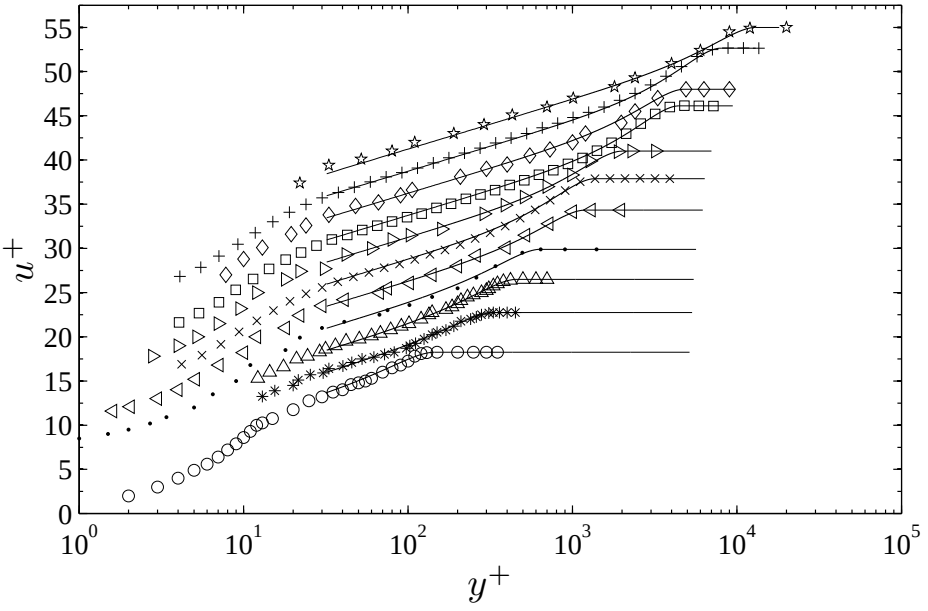

Figure 2: Turbulent boundary layer profiles from experimental data fitted to eq. 8. Symbols as in table 1.

to assess the quality of the analytical fit with DNS as compared to experiments.

3.3. Discussion on the velocity profiles

The quality of the predictions is quantified by evaluating the mean square percentage error ϵ for each profile

$$\epsilon = \sqrt{\frac{1}{N}\sum_{i=1}^{N}\left(\frac{u_a^+ - u_{ex}^+}{u_{ex}^+}\right)^2} \tag{28}$$

where u_a^+ is the predicted value and u_{ex}^+ is the corresponding experimental value for a given y_i^+ in a discretized velocity profile of N points. Similarly, the value u_s^+ is used in expression 28 for the comparison with direct numerical simulations instead of u_{ex}^+. The mean square percentage error ϵ obtained at different Re_θ with u_a^+ evaluated from equation 8 is reported in table 1. The maximum ϵ is 2.05% at $Re_\theta = 31000$. Such error enables the use of eq. 8 to predict the mean streamwise velocity of boundary layers in many common engineering applications, where an error margin of 5% is often acceptable. The experimental data seem to be randomly distributed about the fitted curve with no underlying trend, suggesting that the curve fit has captured most of the u^+ dependence on δ, u_e, u_τ, and Re_θ.

Figure 4 compares velocity profiles obtained using the successive complementary expansion method of section 2.2 against the same experimental data of

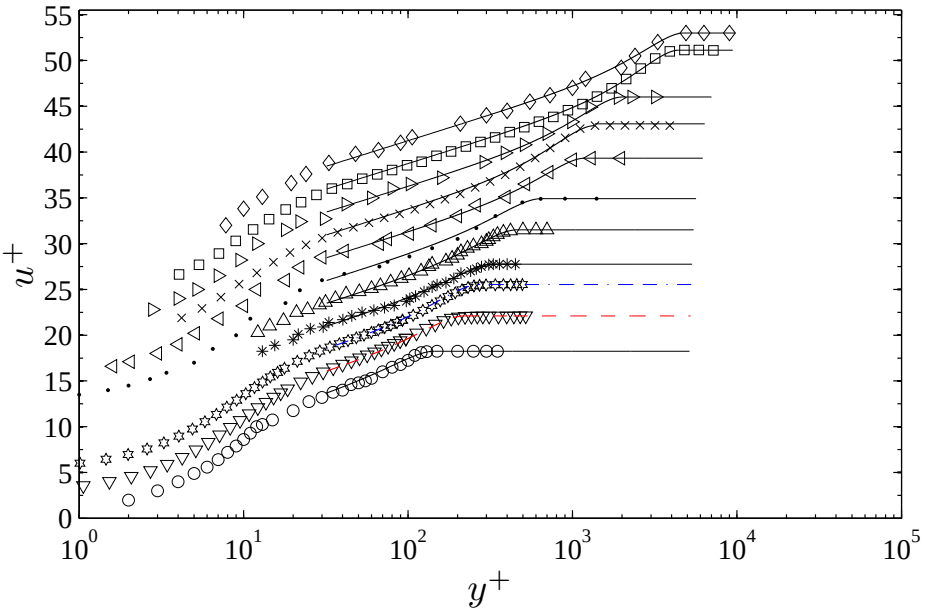

Figure 3: Turbulent boundary layer profiles from experimental and DNS data fitted to eq. 8. Symbols as in table 1.

figure 2. In this application of the successive complementary expansion method, $n = 4$ was used for the numerical prediction of the mixing length in eq. 12. The symbols used in figure 2 are measured values [12, 13, 14, 15] at different Re_θ, labelled as in table 1. The continuous lines show the normalized numerical velocity profiles. For clarity, the same incremental shift of $u^+ = 2.5$ as in figure 2 is applied to all curves. The origin of the ordinate of figure 4 refers to the $Re_\theta = 300$ profile. Figure 4 shows that the complementary expansion method of section 2.2 produces a full velocity profile down to the wall. In the outer layer, the complementary expansion method captures the Reynolds number dependent transition between the log-law and the constant free-stream velocity for most of the curves. The free-stream velocity at $Re_\theta = 22845$, 12663 and 3654 appear to be under-predicted. This is confirmed by the corresponding numerical mean square percentage error, ϵ_n, which is computed by evaluating u_a^+ in eq. 28 using the successive complementary expansion method. The ϵ_n at $Re_\theta = 22845$, 12663 and 3654 are higher than at some of the other Reynolds numbers, due to the difference in the normalized free-stream velocity between experiment and prediction. Figure 5 captures the good agreement of the profiles obtained from the successive complementary expansion method against the DNS profiles. Whereas, in general, the error from the numerical velocity profile is higher than that from the analytical profile, it is within the range for which the predictions can be used for engineering accurate predictions.

The difference between the normalized free-stream velocity from experiment

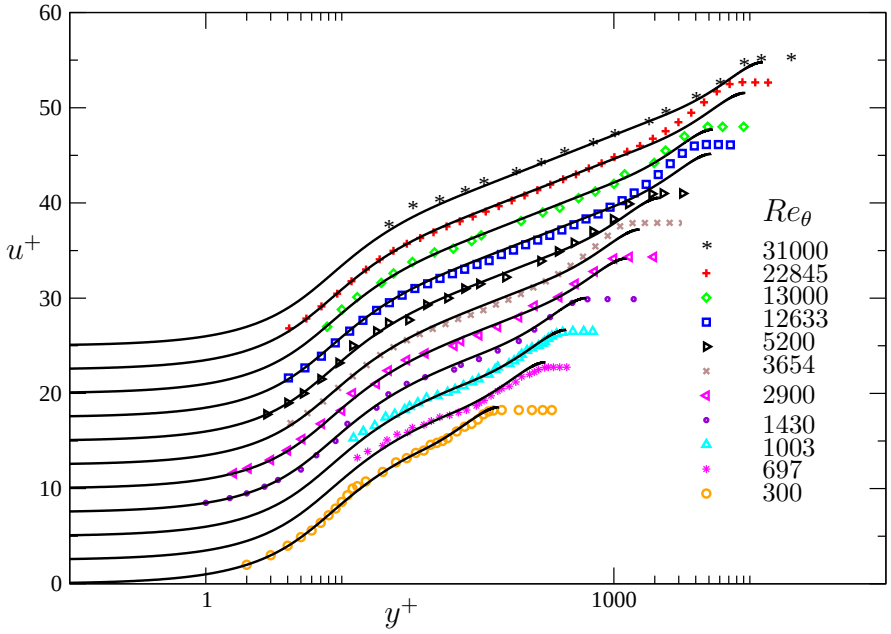

Figure 4: Turbulent boundary layer profiles fitted by the complementary expansion method ($n = 4$). Symbols as in table 1.

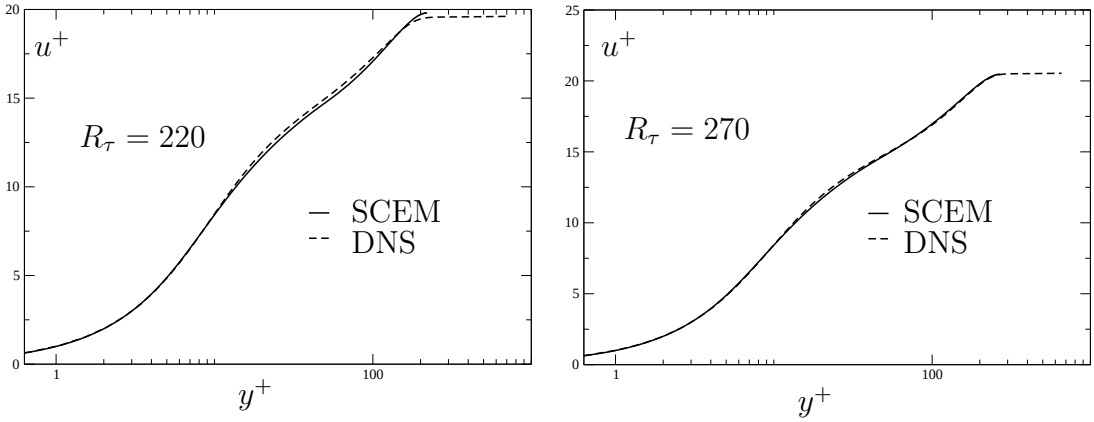

Figure 5: Turbulent boundary layer profiles, comparison between DNS and the complementary expansion method ($n = 4$).

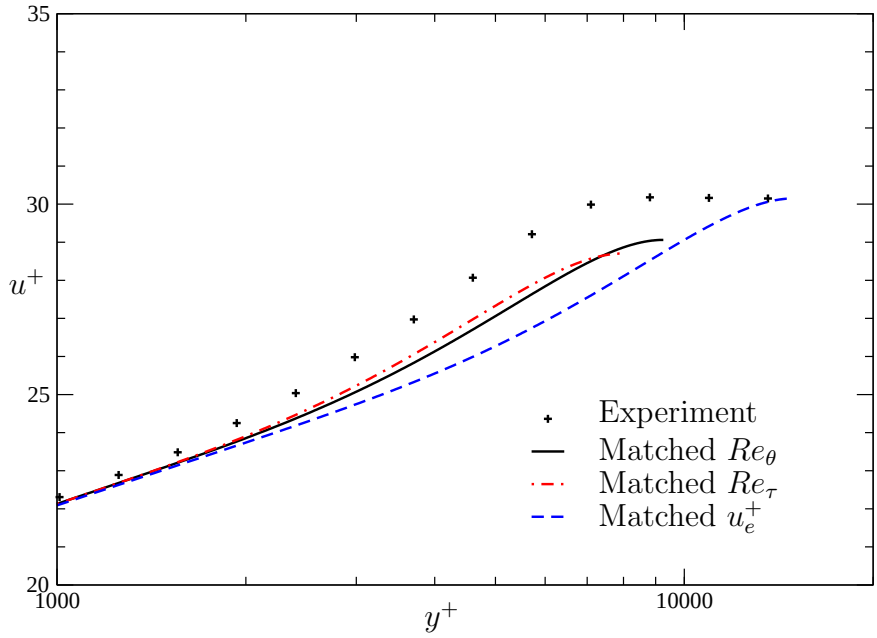

Figure 6: Outer layer profile fitted by the complementary expansion method. $Re_\theta = 22845$. (+) experiment, (−) successive complementary expansion method.

and from the successive complementary expansion method is further investigated in figure 6, where the outer layer portion of the predicted velocity profile at $Re_\theta = 22845$ is re-plotted on a larger scale. The continuous black line is the numerical prediction obtained by matching the experimental value of Re_θ in the matched complementary expansion, the red dash-dot line is obtained by matching the experimental value of Re_τ and the dashed blue line shows the predicted profile with a matched normalized free-stream velocity u_e^+. Matching the experimental Reynolds numbers seems to give similar profiles irrespective of whether the target Reynolds number is defined with respect to the outer scaling variables $u_e\theta/\nu_l$ or the inner scaling variables $u_\tau\delta/\nu_l$. Fitting the outer profile by imposing the normalized free-stream velocity u_e^+ seems to over-predict the boundary layer thickness, leading to a coarser agreement with experiment compared to the numerical predictions obtained by matching the profile Reynolds number.

This paper has not attempted to predict the time-averaged velocity profiles of boundary layers at $Re_\tau < 300$ using the matched complementary expansion method. In this method, u_e^+ is obtained by matching the outer region velocity profile to the inner region velocity profile in the logarithmic layer. At $Re_\tau < 140$, an overlap region in the form of a logarithmic layer is no longer present, which prevents the method form evaluating u_e^+. Here the matched complementary expansion method in its present formulation has reached its lower Re_τ applica-

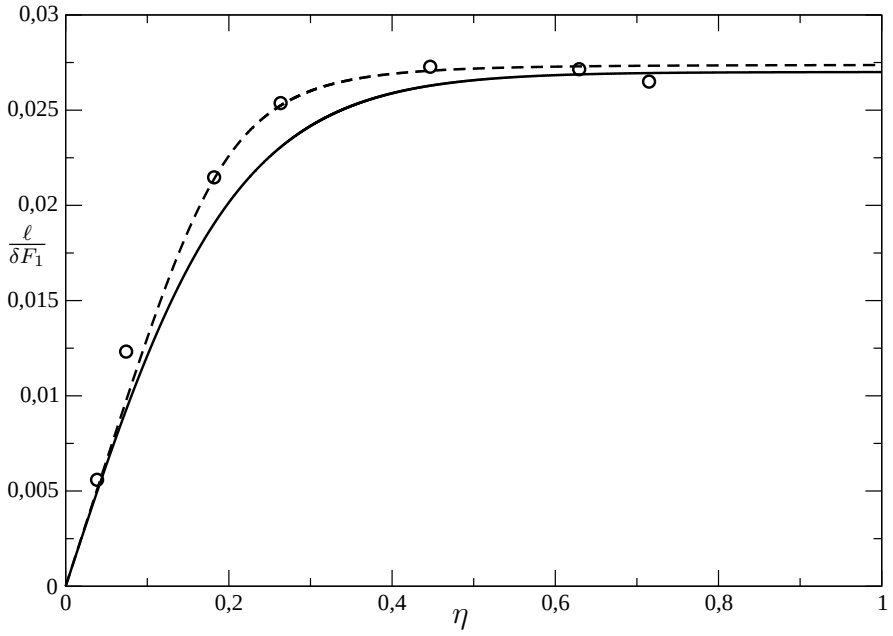

Figure 7: Normalized mixing length $\ell/(\delta F_1)$ versus normalized distance from the wall η. ($\circ$) experiment [17] at $Re_\tau = 1540$, ($--$) matched complementary expansion at $Re_\tau = 1000$ with $F_1 = 3.1479$ from eq. 11, ($-$) matched complementary expansion at $Re_\tau = 1000$ with $F_1 = 3.1044$ from eq. 12 ($n = 4$).

bility limit.

3.4. The shear stress profile

Figure 7 compares the normalized mixing length distribution across a zero-pressure gradient boundary layer with $\ell(\eta)$ obtained from measurements at $Re_\tau = 1540$ by Klebanoff [17], reported in Hinze [18]. The $\ell(\eta)$ distribution from equation 11 is shown by the continuous line while the dashed line shows the distribution from equation 12 with $n = 4$. At this Reynolds number, there appears to be a good improvement in the predicted mixing length using the new formulation. No effort has been made to further optimize $n \in \Re$ by adding decimal digits. Figure 8 shows the profile of the normalized eddy viscosity $\nu_t/(u_\tau F_1 \delta)$ across the same zero pressure gradient boundary layer of figure 7, where $\nu_t = \tilde{F}^2 \ell |\partial u/\partial y|$. The symbols are from the same experiment [17] as in figure 7 (open circles) to which further measurements by Townsend [19] at $Re_\tau = 2775$ have been added (open squares). Using the mixing length model of Michel et al. [10], eq. 11, under-predicts the eddy viscosity, as shown by the continuous line, whereas a better fit is achieved by using eq. 12. As a numerical experiment, the target Reynolds number in the successive complementary expansion method was varied over the range $1000 \leq Re_\tau \leq 2775$ and was found to have very little

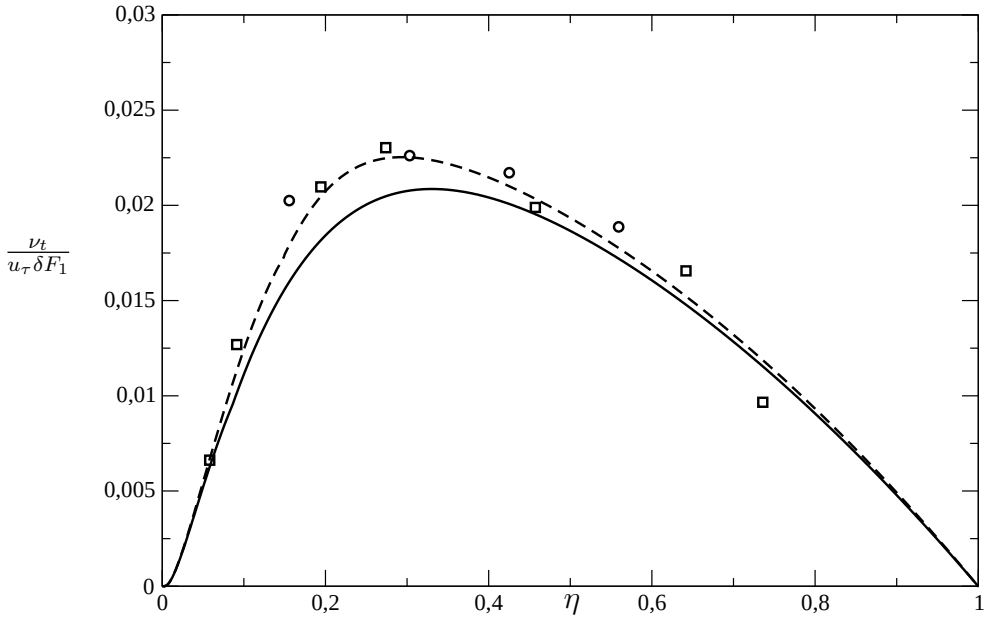

Figure 8: Normalized eddy viscosity $\frac{\nu_t}{u_\tau \delta\ F_1}$ versus normalized distance from the wall η. ($\circ$) experiment [17] at $Re_\tau = 1540$, ($\square$) experiment [19] at $Re_\tau = 2775$, ($--$) matched complementary expansion at $Re_\tau = 1000$ with $F_1 = 3.1479$ from eq. 11, ($-$) matched complementary expansion at $Re_\tau = 1000$ with $F_1 = 3.1044$ from eq. 12 ($n = 4$).

effect on the predicted normalized ν_t, which is also the trend in experiment [17, 19].

4. Adverse pressure gradient boundary layer

4.1. Analytical, numerical and Direct Numerical Simulation results

The methods presented in section 2 are now tested against direct numerical simulation data in order to assess the accuracy for the predictions of non-zero pressure gradients boundary layer mean turbulent velocity profiles. Let consider the Clauser parameter

$$\beta_c = \frac{\delta_1}{u_\tau}\frac{dp}{dx} \tag{29}$$

The values in table 3 are the ones reported in the numerical work [16] for a low adverse pressure gradient (APG1, $\beta_c = 0.24$) and a moderate (APG2, $\beta_c = 0.65$) adverse pressure gradient, respectively. Again, Π has been obtained by fitting eq. 8 using the least squares fit. Results are plotted in figure 3 where the analytical mean velocity profiles for the low adverse pressure gradient (magenta dashed line), the moderate adverse pressure gradient (dashed line) and the zero pressure gradient (blue dashdotted line) are shown in between the experimental zero pressure gradient profiles. The curve fit captures most of the u^+ dependence

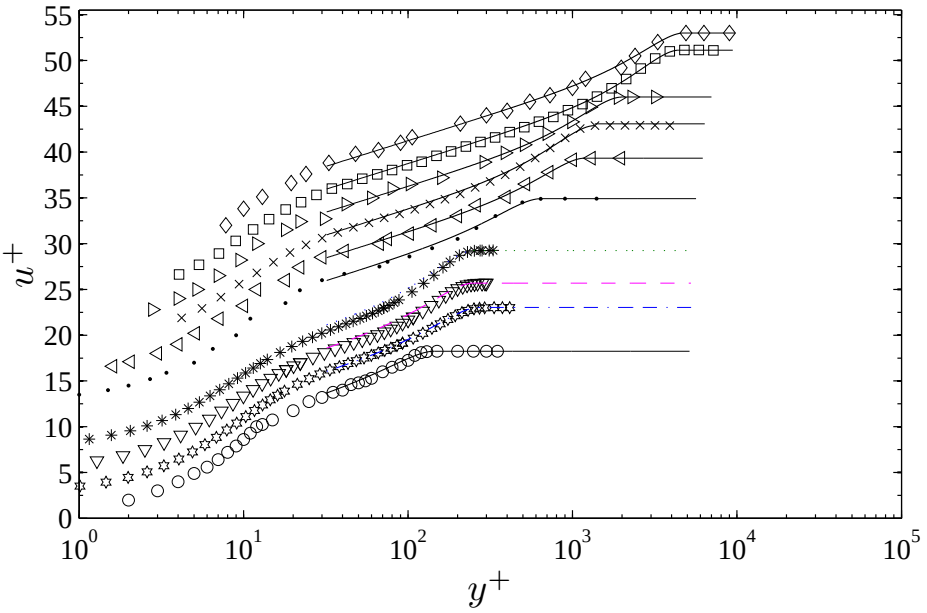

Figure 9: Adverse pressure gradient turbulent boundary layer profiles fitted to eq. 8. Symbols as in table 3.

DNS	β_c	Re_θ	Re_τ	u_s^+	Π	$100 \times \epsilon$	Symbol	$(Re_\tau)_\mathrm{n}$	$(u_e^+)_\mathrm{n}$	$100 \times \epsilon_\mathrm{n}$
APG1	0.24	606	251	20.60	0.385	0.30	$*$	250	21	1.9
APG2	0.65	681	251	21.70	0.455	1.99	$\triangledown$	250	22.3	2.7

Table 3: DNS velocity profiles at low (APG1) and moderate (APG2) adverse pressure gradient.Right-hand side of the table : $n = 24$ in equation 12.

on δ, u_e, u_τ, and Re_θ. The profiles obtained by the asymptotic calculation are further investigated in sections 4.2 and 4.3.

4.2. Determination of Re_τ

Evaluation of the non dimensional parameter Re_τ from DNS data is non trivial. That coincides with the value of y^+ if one of the following is verified:

1. the velocity profile u^+ is zero with respect to y^+,
2. the turbulent shear stress (eq. 16) $\tau^+ = 0$,
3. the non-dimensional turbulent viscosity is zero.

The two first definitions provide the same value of R_τ. The nondimensional turbulent viscosity is given by

$$\frac{\tau^+}{\frac{du^+}{dy^+}} = Re_\tau \frac{\nu_t}{u_\tau \delta} \tag{30}$$

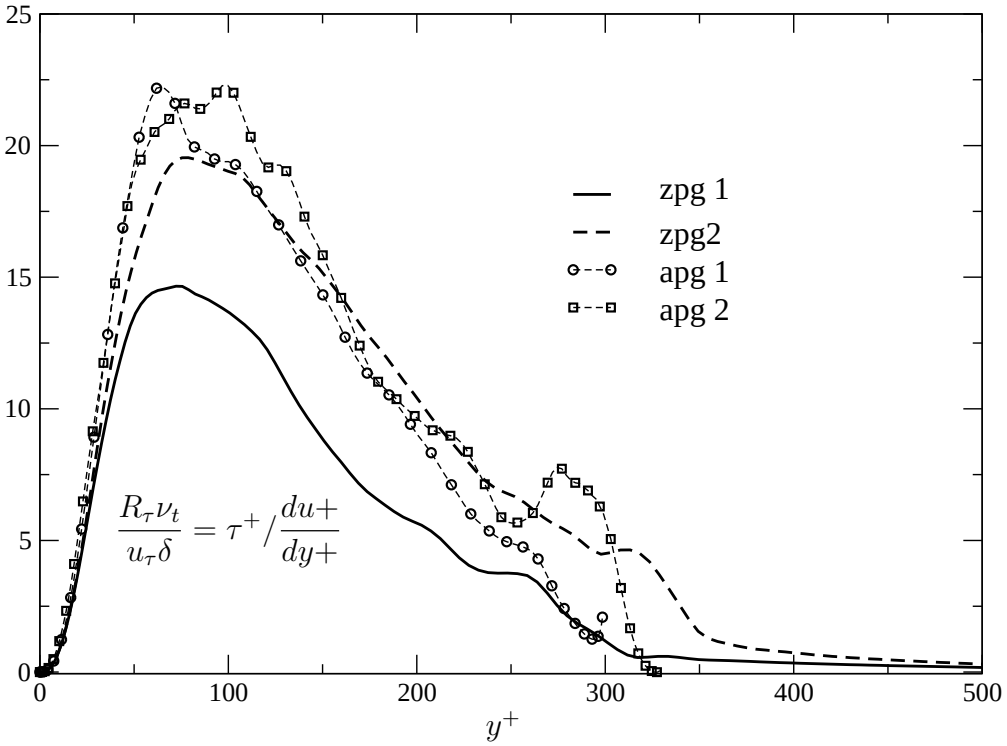

Figure 10: DNS analysis : $\tau^+ / \frac{du^+}{dy^+} = Re_\tau \frac{\nu_t}{u_\tau \delta}$.

It is numerically equivalent to the edge of the boundary layer when $\tau^+ \to 0$ and $\frac{du^+}{dy^+} \to 0$. In figure 10 is shown the function $\tau^+ / \frac{du^+}{dy^+}$, obtained from the DNS computations of [16]. A hump in the region $R_\tau \in [250, 300]$ leads to an overestimation of the R_τ value with respect to the definition 1 and 2. The authors finally remark that the DNS computational domain is approximately as large as the maximum value of y^+ in figure 10, therefore the hump could be a boundary effect of the numerical domain.

4.3. Sensitivity analysis on n

Figure 11 shows the turbulent velocity profiles in presence of a low (figure 11 (a)) and a moderate (figure 11 (b)) adverse pressure gradient, according to table 3. For the asymptotic calculation, two values of the constant n in the mixing length model are tested. These are $n = 24$ and $n = 4$. Both cases seem to show weak dependence of factor n on the velocity profile. However, a deeper analysis on the nondimensional shear stress and the non dimensional turbulent viscosity shows that increasing n improves the agreement between DNS results and the asymptotic approach. A slope mismatch between the asymptotic and

the DNS profile remains, regardless of the n value. To this extent, an inproved multi-parameter mixing length model could be designed to better fit the non dimensional turbulent shear stress.

5. Conclusions

Numerical and analytical methods for obtaining the time-mean velocity profiles of a turbulent boundary layer are presented and validated against experimental data and direct numerical simulation results.

The analytical method is an extension to the law of the wake by Coles [6] that matches both the free stream velocity and the velocity gradient at the boundary layer edge. The method is shown to predict the outer region of turbulent boundary layers rather well for zero streamwise pressure gradient test cases over the Reynolds number range $300 \leq Re_\theta \leq 31000$, with a maximum mean square percentage error of 2.05%.

The authors propose a modification to the successive complementary expansion numerical method in Cousteix & Mauss [7], with a new blending function for the mixing length in the outer region. Comparison against experimental data shows that the new blending function improves the prediction of the mixing length and of the eddy viscosity in outer region of a zero pressure gradient boundary layer. The new method is validated against experimental and direct numerical simulation velocity profile data over the Reynolds number range $300 \leq Re_\theta \leq 31000$ under zero streamwise pressure gradient and found to achieve engineering accurate predictions. The new blending function introduces an additional adjustable parameter $n \in \Re$ in the model that can undergo a more extensive calibration over a wider experimental data-set to further improve the predictions. The results of the asymptotic and numerical results in the presence of adverse pressure gradient show a good prediction of the velocity profiles. In the asymptotic formulation, the proposed mixing length model provides good agreement on velocity profile. A mismatch of the turbulent viscosity in the log-layer at low R_τ suggests however an improvement of the mixing length model to a multi parameter formulation.

Acknowledgments

This research project has been supported by a Marie Curie Research Training Fellowship of the European Community's Sixth Framework Programme under contract MEST CT 2005 020301. This paper was written with the support of the Invited Professorship scheme of the Université Paul Sabatier, Toulouse.

References

[1] A. Rona, E. J. Brooksbank, Injection parameters for an effective passive control of the cavity flow instability, in: 40th AIAA Aerospace Sciences Meeting & Exhibit, AIAA, Reno, NV, 2002.

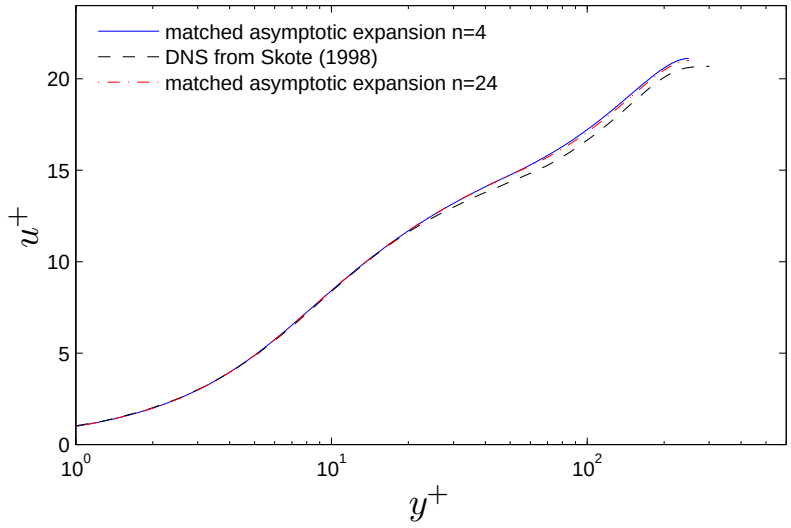

(a) Adverse pressure gradient $\beta_c = 0.24$

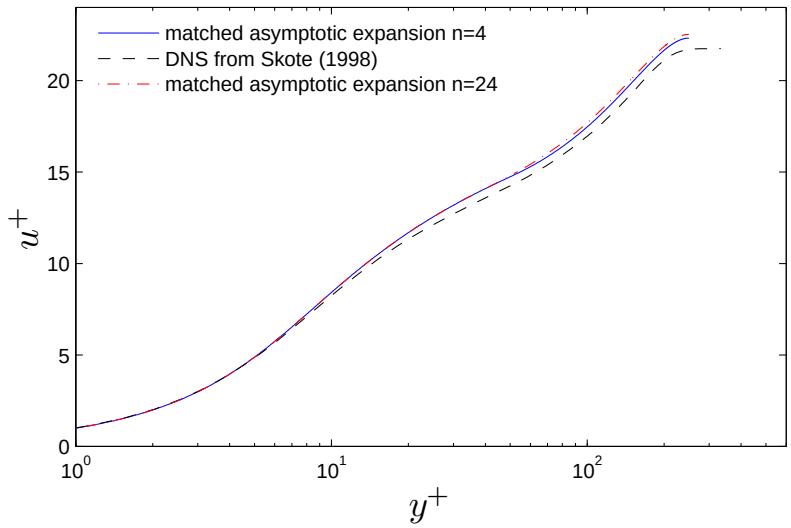

(b) Adverse pressure gradient $\beta_c = 0.65$.

Figure 11: Sensitivity on n. $n = 4$ and $n = 24$.

[2] M. Grottadaurea, A. Rona, Noise sources from a cylindrical cavity, in: 13th AIAA/CEAS Aeroacoustics Conference, no. 2007-3723, AIAA, Rome, Italy, 2007.

[3] M. Grottadaurea, A. Rona, The role of the inflow momentum thickness in subsonic cylindrical cavity noise generation, in: 14th International Congress on Sound and Vibration, no. 165, International Institute of Acoustics and Vibration, Cairns, Australia, 2007.

[4] C. Rowley, T. Colonius, A. Basu, On self-sustained oscillations in two-dimensional compressible flow over rectangular cavities, J. Fluid Mechanics 455 (2002) 315–46.

[5] D. Wilcox, Turbulence modeling for CFD, 2nd Edition, D. C. W. Industries, 2002.

[6] D. Coles, The law of the wake in the turbulent boundary layer, J. Fluid Mech. 1 (1956) 191–226.

[7] J. Cousteix, J. Mauss, Asymptotic analysis and boundary layers, Springer-Verlag, Berlin Heidelberg, 2007.

[8] L. Prandtl, Bericht über untersuchungen zur ausgebildeten turbulenz, Z. Angew. Math. Mech. 5 (1925) 136–139.

[9] E. R. Van Driest, On dimensional analysis and the presentation of data in fluid-flow problems, ASME Journal of Applied Mathematics 13 (1) (1946) 34–40.

[10] R. Michel, C. Quémard, R. Durant, Application d'un schéma de longueur de mélange à l'étude des couches limites turbulentes d'équilibre, Technical Note 154, ONERA (1969).

[11] J. Cousteix, Outer boundary layer self-similar solution, private communication (2009).

[12] P. R. Spalart, Direct simulation of a turbulent boundary layer up to $r_\theta = 1410$, J. Fluid Mech. 187 (1988) 61–98.

[13] L. Erm, P. N. Joubert, Low-reynolds-number turbulent boundary layers, J. Fluid Mech. 230 (1991) 1–44.

[14] D. B. De Graaff, J. K. Eaton, Reynolds-number scaling of the flat-plate turbulent boundary layer, J. Fluid Mech. 442 (2000) 319–346.

[15] J. M. Österlund, Experimental studies of zero pressure-gradient turbulent boundary layer flow, Phd thesis, Royal Inst. Techn., KTM, Stockholm (1999).

[16] M. Skote, D. S. Henningson, Direct numerical simulation of self-similar turbulent boundary layers in adverse pressure gradients, Flow, Turb. Comb. 60 (1998) 47–85.

[17] P. S. Klebanoff, Characteristics of turbulence in a boundary layer with zero pressure gradient, Technical Note 3178, National Advisory Committee for Aeronautics (NACA) (1954).

[18] J. O. Hinze, Turbulence, McGraw-Hill, New York, 1975.

[19] A. A. Townsend, The structure of the turbulent boundary layer, Mathematical Proceedings of the Cambridge Philosophical Society 47 (2) (1951) 375–395.